Overlap Concentration in Salt-Free Polyelectrolyte Solutions

Jonathan A. Bollinger,[†] Gary S. Grest,[†] Mark J. Stevens[*,†] and Michael Rubinstein[*,‡]

† *Sandia National Laboratories, Center for Integrated Nanotechnologies, Albuquerque, NM 87185*

‡ *Mechanical Engineering and Materials Science, Biomedical Engineering, Chemistry, and Physics Departments, Duke University, Durham, NC 27708*

E-mail: gsgrest@sandia.gov

Abstract

For strongly charged polyelectrolytes in salt-free solutions, we use molecular dynamics simulations of a coarse-grained bead-spring model to calculate overlap concentrations c^* and chain structure for polymers containing N=10 to 1600 monomers. Over much of this range, we find that the end-to-end distance R^* at c^* increases faster than linearly with increasing N, as chains at the overlap concentration approach strongly extended conformations. This trend results in overlap concentration c^* decreasing as a stronger function of N than the classical prediction $c^* \sim N^{-2}$. This stronger dependence can be fit either by a logarithmic correction to scaling or by an apparent scaling $c^* \sim N^{-m}$, with $m > 2$.

Introduction

Strongly-charged polyelectrolytes comprise an important class of polymers, including biopolymers, such as DNA, and synthetic polymers, such as sodium polystyrene sulfonate (NaPSS). For strongly-charged polyelectrolytes, the Bjerrum length $\ell_B = e^2/\epsilon_{\rm R} k_{\rm B} T$ (where e is electron charge, $\epsilon_{\rm R}$ is relative permittivity, and $k_B T$ is thermal energy) and the charge spacing along the polymer backbone a are comparable, resulting in comparable contributions to the electrostatic and entropic parts of free energy. Thus, strongly charged polyelectrolytes exhibit much more complex behavior as a function of chain length, concentration, and additional parameters such as ionic strength than uncharged polymers. Consequently, the structural and dynamic properties of strongly charged polyelectrolytes are not as well characterized as those of neutral polymers,[1] and remain a continuing challenge for experiments and theory.[2–5]

The overlap concentration c^* that defines a crossover between dilute and semi-dilute solutions is a key quantity for polymeric systems.[6,7] Accurate measurements of the overlap concentration c^* for strongly-charged high molecular weight M_W polyelectrolytes in salt-free solutions remain a major experimental challenge. In x-ray or neutron scattering experiments,[8] c^* is determined as the crossover in the concentration dependence of the position $q_{\rm max}$ of the primary peak in the structure factor $S_{\rm tot}(q)$ between $q_{\rm max} \sim c^{-1/3}$ and $q_{\rm max} \sim c^{-1/2}$. Measuring c^* becomes increasingly difficult for higher molecular weight polyelectrolytes, because their overlap concentration is very low with small signal-to-noise ratio and hard to precisely control ionic conditions. Alternatively, in viscosity experiments, c^* is defined as the concentration at which the specific viscosity $\eta_{\rm sp} \equiv 1$.[9] However, the resulting uncertainty in determination of c^* for high molecular weight polyelectrolytes is very large (up to an order of magnitude) due to the difficulties in controlling the 'zero salt' ionic condition as well as shear thinning effects. It is important to realize that these two measurements of c^* are not equivalent, because scattering measures the static structure of the system while rheology measures the dynamic response of the system. At best, the two methods give the values of c^* that are proportional to each other, but are not nececessarily equal.

An accurate calculation of the overlap concentration c^* for strongly-charged polyelectrolytes remains a challenge for polymer theory. The classical prediction[10] of the end-to-end distance at overlap $R^* \sim N$, leads to the overlap concentration dependence on the degree of polymerization $c^* \sim N^{-m}$ with $m = 2$ that has been typically used in the comparison to experimental data.[1] Scaling models of polyelectrolyte solutions[11,12] predict the same scaling of the overlap concentration. However, this estimate ignores three physical effects important for strongly charged polyelectrolytes. First, the electrostatic energy of a uniformly stretched polyelectrolyte chain of size R with total number of elementary charges Q is not $k_BTl_BQ^2/R$ assumed in the above-mentioned theories, but has an additional logarithmic dependence $k_BTl_BQ^2 \ln Q/R$ on charge, that modifies the N-dependence of the end-to-end distance R^* and the overlap concentration c^*.[13] In addition, for polyelectrolytes with charge separation along the end-to-end vector smaller than the Bjerrum length, counterion condensation is relevant and must be included. The extent of the counterion condensation is determined by the interplay of counterion entropy loss and electrostatic energy gain and results in additional logarithmic corrections of the N-dependence of R^* and c^*. Finally, the conformations of strongly charged polyelectrolytes are highly extended and require treatment of the nonlinear elasticity. Here we provide simulation data for a coarse-grained bead spring model to test these theoretical issues related to strongly charged polyelectrolytes over a wide range of chain lengths.

Simulation Method

Molecular dynamics simulations provide detailed structural information sufficient to determine c^*, but calculations for large N have to date been beyond computational capability. Here, we present results for c^* for chain lengths up to $N = 1600$ using a standard coarse-grained model of salt-free polyelectrolyte solutions. Each simulation comprises M chains of N beads of unit mass and charge e, which interact via the Lennard-Jones (LJ) potential

cut and shifted at $r_c = 2^{1/6}\sigma$ and the Coulomb potential (see Fig. 1). [14] These are fully compensated with counterions that are explicitly treated as charged LJ beads. Simulations include between $M = 800$ chains (for small N and high c) to $M = 27$ chains (for large N and low c). We choose parameters that correspond to a generic strongly charged polyelectrolyte, where $\ell_B = 1\sigma$ and $a \simeq 1\sigma$ (σ is the monomer bead size). This is about the ratio of nucleic acid polymers and comparable but somewhat weaker charged than a polyelectrolyte like sodium polystyrene sulfonate (NaPSS), where $\ell_B/a \approx 2.8$. The dielectric constant of water changes with temperature keeping ℓ_B almost constantwith just a 15% change over the practical range of temperatures. We also simulate corresponding neutral polymer systems, which include NM uncharged LJ beads in addition to polymers.

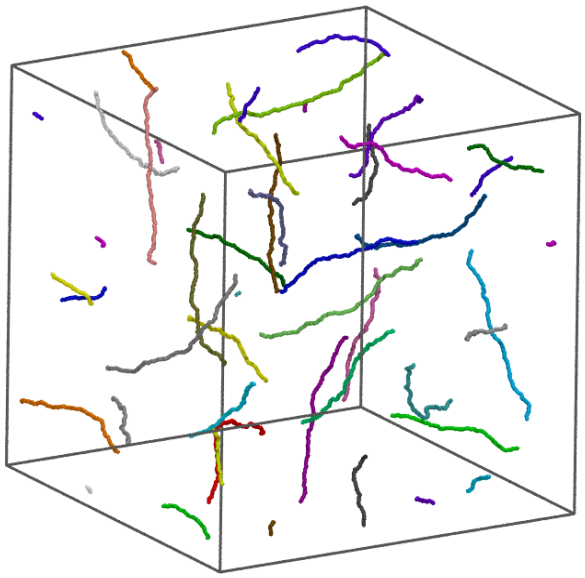

Figure 1: Image of the $N = 800$ system at $c = 10^{-5}\sigma^{-3}$ showing only the polymers with each one a different color. $c^* = 4.1 \cdot 10^{-6}\sigma^{-3}$. The bead size has been scaled up by about a factor of 5 to make the chains visible.

Each chain contains N monomers connected with a FENE bond with spring constant $k = 30\epsilon/\sigma^2$ and maximum extent $R_0 = 1.5\sigma$, where ϵ is the LJ energy and σ is the LJ diameter. A cosine angle potential with spring constant of $k_\theta = 1.5\epsilon$ is used to give the chains an intrinsic Kuhn length $= 2.9\sigma$ to match previous neutral polymer simulations. The solvent is treated as a dielectric continuum.[14] A particle-particle particle mesh Ewald

method[15] is used to evaluate the Coulomb interactions with a real space cutoff of 6.5σ and precision 10^{-3}. The temperature is fixed at ϵ/k_B using a Langevin thermostat with damping frequency $0.01\tau^{-1}$. The timestep is 0.01τ when using a single time step integrator, where τ is the LJ time unit. At low densities, the rRESPA multi-timescale integrator[16] is used with a time step of 0.01τ for bonds, angles and a time step of 0.02τ for the long range part of the electrostatic interactions. Total simulation times were at least 400,000 τ.

Results

The overlap (monomer) concentration c^* was calculated using two methods: (1) the method used in scattering experiments based on the peak position $q_{\max}$ in $S(q)$ and (2) a dense-packing condition. Calculation of the overlap concentration c^* from the peak $q_{\max}$ in the structure factor was done for several values of $N \leq 800$. Figure 2 shows $S(q)$ at a subset of the concentrations at $N = 400$, which shows the resolution of the peak position. To span the wide range of q values this axis is on a log scale, which means that the peaks at low c are on a finer scale than those at high c. Overall, the resolution of $q_{\max}$ is not an issue for the N that we can simulate sufficient number of concentrations. The requirement to simulate many concentrations below $10^{-6}\sigma^{-3}$ makes this method currently not feasible for $N > 800$.

In Figure 3, $2\pi/q_{\max}$ is plotted as a function of concentration for 5 values of N from 50 to 800 showing the crossover from $q^{1/3}$ to $q^{1/2}$ scaling as concentration increases. To obtain c^*, the crossover point is determined by fitting the data in dilute solutions to

$$q_{max} = 2\pi(c/A(N)N)^{1/3} \tag{1}$$

and in semi-dilute solutions

$$q_{\max} = 2\pi(cb/B(N))^{1/2}, \tag{2}$$

where $b = 0.97\sigma$ is the bond length. The intersect of these functions at overlap concentra-

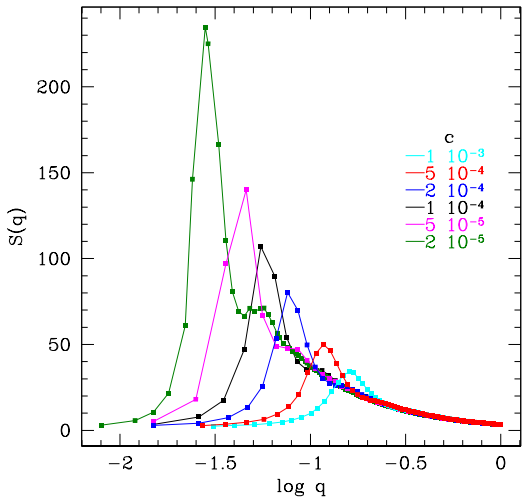

Figure 2: The total scattering function $S(q)$ for $N = 400$ at various c.

tion $c^* = B(N)^3/(N^2b^3A(N)^2)$. The surprising finding was that the deviation of the N-dependence of the overlap concentration from the classical N^{-2} dependence is due largely to the weak increase of the dilute solution coefficient $A(N)$ with increasing N (see plot of $A(N)$ versus N in insert of Fig. 3), while the semidilute solution coefficient $B(N) = 1.59 \pm 0.04$ is constant. This unexpected result suggests that the extension of the chain along its contour in semidilute solutions $1/B(N) = L/bN$ is both concentration and N-independent with q_{max} following the classical $c^{1/2}$ prediction with no corrections, while if the peak position in dilute solutions related to the separation between chains — it does not follow the expected $(c/N)^{1/3}$ dependence, but has an additional $A(N)^{-1/3}$ correction.

In the second method, the overlap concentration is defined as $c^* = 0.64N/(\pi R^{*3}/6)$, where R^* is the root mean squared end-to-end distance of the chain at c^*. These two methods provide similar information because for $c \leq c^*$, $q_{\max}$ corresponds to the center-of-mass separation distance between chains, and the overlap occurs when this separation is proportional to R^*. In tables 1 and 2 we present the overlap concentrations for the charged and neutral systems, respectively. Within the uncertainties, these two methods are in very good agreement for $N \leq 200$. For $N = 400$ and 800, c^* from q_{max} is larger than from the

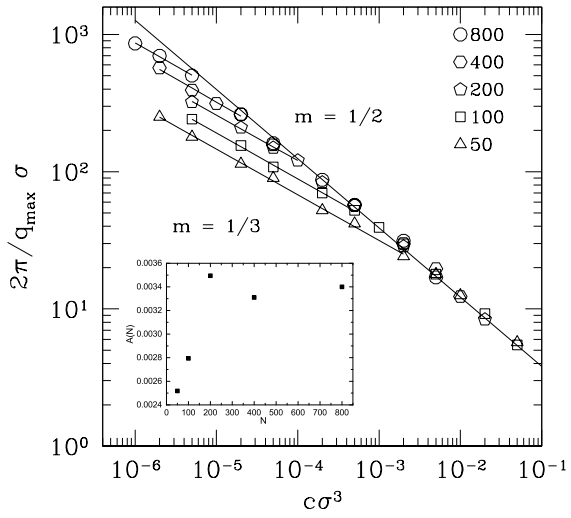

Figure 3: Peak position q_{max} in the structure factor $S(q)$ as a function of concentration for 5 values of chain length N showing transition from scaling of $q_{max} \sim c^m$ with exponent $m = 1/2$ to $1/3$. Insert shows $A(N)$ vs. N. For $m = 1/2$, the line is for $N = 200$.

packing, due in large part, from the fact that the data for q_{max} for $c < c^*$ is not very far below $< c^*$, resulting in an over estimate of c^*. Below we use c^* values from the dense-packing definition unless otherwise noted.

Table 1: Overlap concentrations calculated using R and $q_{\max}$ for polyelectrolyte systems.

N	$R^*(\sigma)$	$c^*(\sigma^{-3})^a$	$c^*(\sigma^{-3})^b$	$A(N)$	$B(N)$
10	5.4	$7.8 \cdot 10^{-2}$			
20	9.8	$2.6 \cdot 10^{-2}$			
50	24.0	$4.4 \cdot 10^{-3}$	$4.0 \cdot 10^{-3}$	0.0025	1.56
100	52.4	$8.5 \cdot 10^{-4}$	$8.2 \cdot 10^{-4}$	0.0028	1.58
200	121	$1.4 \cdot 10^{-4}$	$1.3 \cdot 10^{-4}$	0.0035	1.48
400	281	$2.2 \cdot 10^{-5}$	$3.6 \cdot 10^{-5}$	0.0033	1.68
600	451	$8.0 \cdot 10^{-6}$			
800	623	$4.1 \cdot 10^{-6}$	$5.7 \cdot 10^{-6}$	0.0034	1.64
1200	973	$1.6 \cdot 10^{-6}$			
1600	1315	$8.6 \cdot 10^{-7}$			

[a]Calculated from R; [b]Calculated from $q_{\max}$

The concentration dependence of the average end-to-end distance R (divided by N, which is proportional to the chain contour length $\sim Nb$) for $N = 50$ and 800, with red arrows marking the overlap concentrations is shown in Fig. 4. As expected, R is constant at con-

Table 2: Overlap concentrations calculated using R for neutral systems.

N	$R^*(\sigma)$	$c^*(\sigma^{-3})$
10	4.9	$1.0 \cdot 10^{-1}$
50	13.1	$2.7 \cdot 10^{-2}$
200	30.1	$9.0 \cdot 10^{-3}$
800	68.8	$3.0 \cdot 10^{-3}$
1600	101	$1.9 \cdot 10^{-3}$
3200	155	$1.0 \cdot 10^{-3}$

centrations below c^* for neutral polymers. However, the two charged cases display different behavior depending on N. The charged chains at $N = 50$ are not as strongly extended ($R^*/(N\sigma) \simeq 0.5$) at overlap and continue to stretch considerably upon dilution below overlap as was observed in earlier simulations.[13,14] Here, the prevailing interpretation has been that the chemical potential of the dissociated counterions decreases logarithmically with decreasing polymer concentration, thereby reducing the concentration of the counterion cloud near the polymer. Thus, the compensation of the effective polymer charge decreases resulting in polyelectrolyte extension upon dilution. Longer polyelectrolyte chains with $N = 800$ are highly extended at overlap ($R^*/(N\sigma) \simeq 0.8$ and see Fig. 1) and therefore do not significantly stretch upon further dilution (see also Fig. 6). This implies that once N is large enough, the counterion chemical potential is low enough that most counterions are already far from the chains and polyelectrolytes are extended at overlap almost as much as they would be without counterions. Thus, lowering the concentration below c^* does not significantly increase effective polyelectrolyte charge nor the strength of intramolecular electrostatic repulsion of these long chains. As evident from Fig. 1 we find no orientational correlation among the chains at any N.

The calculated overlap concentrations are plotted comparing charged and neutral values in Fig. 5. Notably, for polyelectrolytes we observe an effective power law dependence $m > 2.0$ for both methods. Specifically, $m = 2.5$ determined from packing criterion and $m = 2.4$ determined from the peak in $S(q)$. As shown in the Fig. 5, these power laws are clearly distinguishable from the dependencies previously predicted by Flory theory ($c^* \sim N^{-2}$)[10]

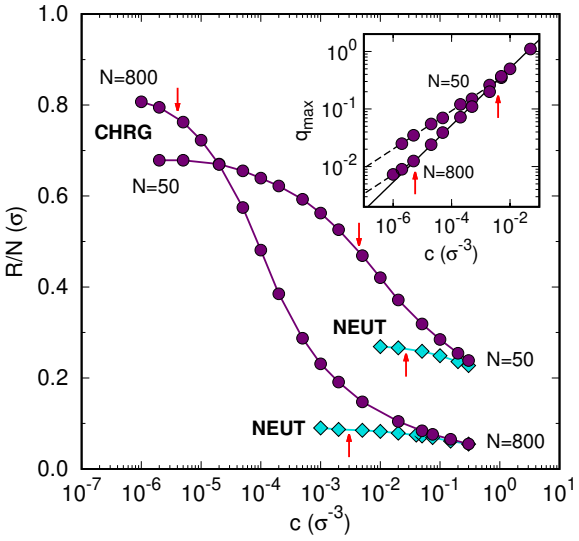

Figure 4: Concentration dependence of the average end-to-end distances normalized by the chain length R/N for neutral (diamonds) and charged (circles) chains of size $N = 50$ and 800. Arrows highlight overlap conditions c^* and R^*/N. Inset: peak position $q_{\max}$ in structure factor $S(q)$ for charged chains from Fig. 1 as a function of polymer concentration showing identification of c^* (red arrows).

or the modified scaling model ($c^* \sim N^{-2}/\ln N$).[13] The data is consistent with a stronger logarithmic correction $c^* \sim N^{-2}/(\ln N)^{\alpha}$ with exponent $\alpha \simeq 3$. The overlap concentration obtained from the neutral simulations follows the scaling with an exponent of 0.79, which is close to the theoretically predicted power-law scaling exponent 0.76.[1]

Insight into the dependence of c^* on N can be obtained by examining R^*, the chain size at the overlap concentration, as a function of N as shown in Fig. 6a as well as a log-log plot in Fig. 6b. For the neutral systems, $R^*/(N\sigma)$ monotonically decreases across all N, as expected for chains simply exhibiting self-avoiding random walks with $R^*/\sigma \sim N^{0.59}$ consistent with $c^* \sim N^{-0.79}$ scaling in Fig. 5. In contrast, for charged systems, we observe a non-monotonic trend in $R^*/(N\sigma)$, where R^*/σ does not scale linearly with N (a linear dependence would be expected from Flory or simple scaling theory). For $N \leq 100$, the magnitude of $R^*/(N\sigma)$ is roughly 0.5, indicating that the chains are not highly extended. For example, the snapshot in Fig. 6 for an $N = 50$ chain just above overlap shows significant bends. For $100 < N \leq 1600$, the magnitude of R^*/N increases with N and eventually results

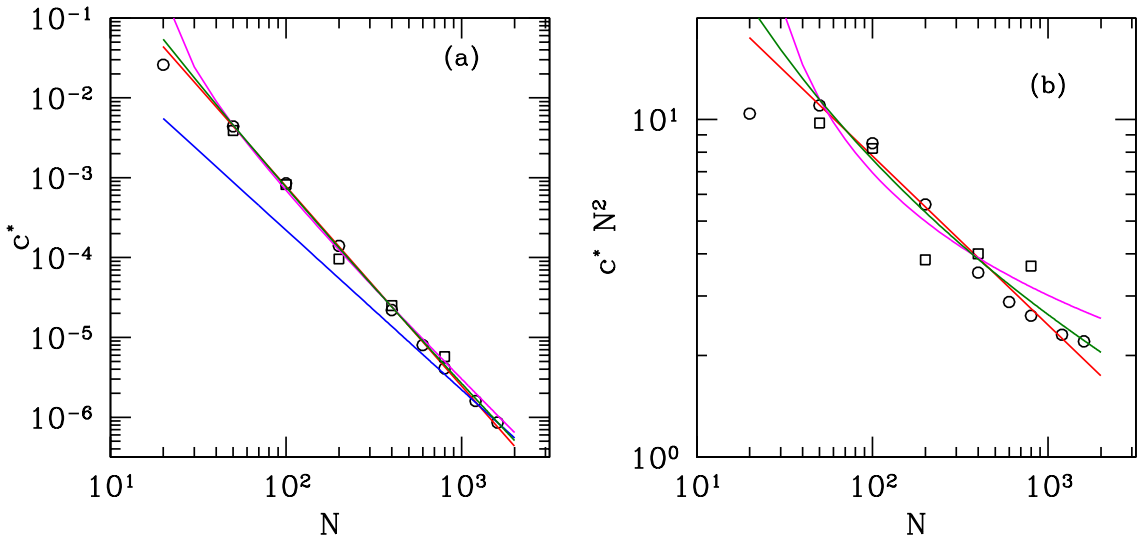

Figure 5: Overlap concentration c^* as a function of number of monomers in a chain of length N. The circles are from the R^* overlap concentration and the squares are the c^* obtained from $q_{\max}$. In (a) and (b), the red line is a least squares fit for the power law $c^* \sim N^{-m}$ to the R^* overlap concentrations for $N > 20$ yielding exponent $m = 2.5$. The blue line in (a) is the $c^* \sim N^{-2}$ scaling going through the $N = 1600$ point. In (a) and (b) the magenta line is the best fit to $c^*N^2 = A_c/\log(N/g)$ with $A_c = 5.3$ and $g = 17.2$ for c^* obtained from the overlap condition. The green line is the best fit to $c^*N^2 = A_c/(\log(N/g)^3$ which fits well with $A_c = 101$ and $g = 0.4$.

in highly extended chains exemplified by the $N = 800$ snapshot. This progression from bent to strongly extended conformations at overlap causes the $c^* \sim N^{-m}$ behavior with $m > 2$. This N range with changing $R/(N\sigma)$ is not in the scaling regime and the exponents are simply effective values. Not until large $N \geq 800$, do the chains exhibit sizes comparable to the infinite dilution limit, where counterions do not alter intramolecular electrostatic repulsion. We calculate this infinite dilution limit for $R/(N\sigma)$ (dotted line in Fig. 6) via separate Monte Carlo simulations of single chains without counterions.[17] The trend toward the dilute limit is consistent with the decrease in the fraction of condensed counterions with increasing N.

The polymer structure at all length scales as one approaches c^* can be obtained by analyzing the single-chain form factor $P(q)$ for $N = 50$ and 800 at different concentrations as shown in Fig. 7. At the higher concentrations studied the intramolecular electrostatic

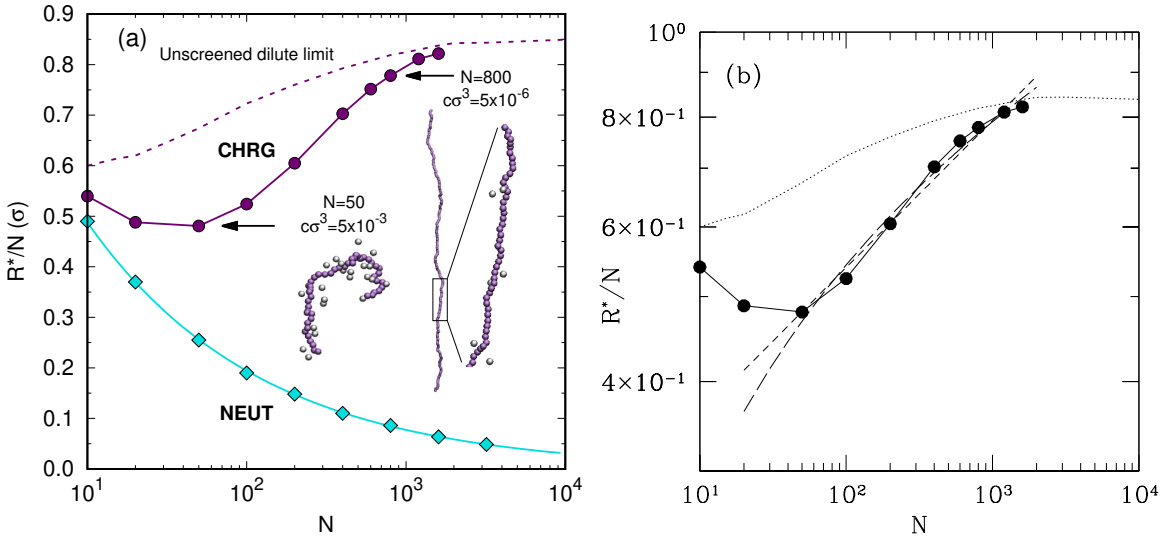

Figure 6: (a) Average end-to-end distances at overlap normalized by number of monomers $R^*/(N\sigma)$ versus N for charged (circles) and neutral (diamonds) simulations. Solid line tracing neutral data is given by $R^*/(N\sigma) = (5/4)N^{-0.40}$. Dotted line traces the sizes $R/(N\sigma)$ of charged chains at infinite dilution condition without counterions. Snapshots show chains at $N = 50$ and 800 (marked with arrows) having $R \approx R^*$ taken from configurations at densities close to overlap ($c^*\sigma^3 = 4.4 \cdot 10^{-3}$ and $4.0 \cdot 10^{-6}$ for $N = 50$ and 800, respectively). Chain beads are shown in purple, while counterions within 3σ of the chains are shown in gray. (For visibility of the full $N = 800$ chain, we decrease bead diameter by 4x and do not show the counterions.) The zoomed-in portion of the $N = 800$ chain spans a representative 50-bead region. (b) Log-log plot of $R^*/(N\sigma)$ vs. N for polyelectrolyte data compared to scaling relations. The dotted line traces the sizes $R/N\sigma$ of charged chains at infinite dilution condition without counterions. For $N > 20$, the short dashed line is the relation $R^*/(N\sigma) = (N/g)^\alpha$ with fit parameters $g = 3990$ and $\alpha = 0.167$, and the long dashed line is $R^*/(N\sigma) = A\log(N/g)$ with $A = 0.25$ and $g = 0.64$.

interactions are compensated by counterions and charged chain $P(q)$ profiles resemble those of neutral chains at c^* where $P(q) \sim q^{-1/\nu}$ and $\nu \approx 0.6$. For even higher concentrations, both are expected to cross-over to random walks with $\nu = 1/2$. At other (lower) concentrations, two distinct components of $P(q)$ appear: a high-q range with $P(q) \sim q^{-1/\nu}$ with $\nu > 0.90$ (i.e., strongly extended conformations) and a low-q range with $0.6 \leq \nu \leq 0.9$. Defining q_r as the crossover between the high and low q regimes, $L_r = 2\pi/q_r$ is the size of extended chain segments that form larger scale conformations with an effective fractal dimension (the low-q $1/\nu$) that increases with decreasing concentration. For $N = 50$ near c^*, $L_r \approx 15\sigma$,

which corresponds to about three extended segments that bend to result in $R^*/N \approx 0.5$ (see Fig. 6). In contrast, for $N = 800$ near c^*, $L_r \approx 600\sigma$, corresponding to a single extended segment that results in $R^*/N\sigma \approx 0.8$ (see Fig. 6). $P(q)$ for $N = 800$ at c^* in Fig. 7 is almost identical to that at infinite dilution. This latter behavior is general for charged chains at large N: the low-q regime in $P(q)$ disappears at concentrations approaching c^*, and there is a single extended chain regime with $\nu > 0.90$, as assumed in most models of dilute salt-free polyelectrolyte solutions.

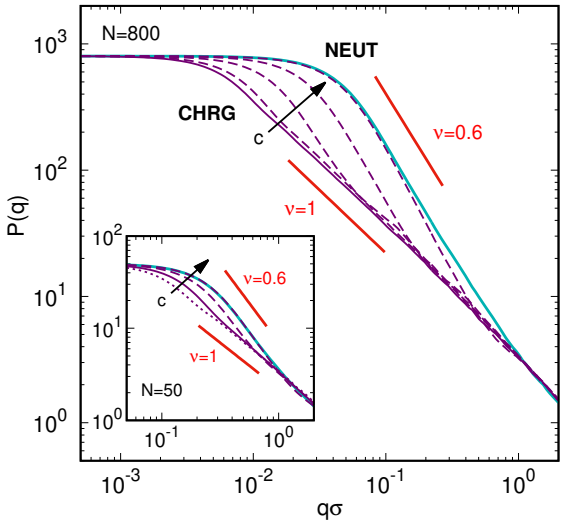

Figure 7: Single-chain form factors $P(q)$ for $N = 800$. Blue line shows $P(q)$ for neutral chains at $c = 5.0 \cdot 10^{-3}\sigma^{-3}$ (closest data above $c^* = 3.1 \cdot 10^{-3}\sigma^{-3}$). Purple lines show $P(q)$ for charged chains, where solid line corresponds to $c\sigma^3 = 5.0 \cdot 10^{-6}$ ($c^*\sigma^3 = 4.0 \cdot 10^{-6}$) and dashed lines to $5.0 \cdot 10^{-5}, 5.0 \cdot 10^{-4}, 5.0 \cdot 10^{-3}$, and $5.0 \cdot 10^{-2}$, respectively. Inset: $P(q)$ for $N = 50$. Blue line show $P(q)$ for neutral chains at $c\sigma^3 = 5.0 \cdot 10^{-2}$ ($c^*\sigma^3 = 2.7 \cdot 10^{-2}$). Purple lines show $P(q)$ for charged chains, where solid line corresponds to $c\sigma^3 = 5.0 \cdot 10^{-3}$ ($c^*\sigma^3 = 4.4 \cdot 10^{-3}$) and dashed lines to $5.0 \cdot 10^{-2}$ and $2.0 \cdot 10^{-1}$ (left to right). Dotted purple line shows $P(q)$ for dilute conditions $c\sigma^3 = 5.0 \cdot 10^{-6}$. In both panels, solid red lines show power-law scaling for $P(q) \sim q^{-1/\nu}$.

In summary, we have calculated overlap concentrations for strongly-charged polyelectrolytes in salt-free solutions that yield new results not only of the c^* dependence on N but also of chain structure. Over a large range of N, the end-to-end distance R^*/σ at c^* increases faster than linear with N, i.e. the relative chain extension $R^*/(N\sigma)$ is higher at larger N.

This yields an effective scaling of the overlap concentration $c^* \sim N^{-m}$, with $m = 2.4 - 2.5$, for strongly-charged chains for $20 < N \leq 1600$. Alternatively, this stronger dependence can be described as a logarithmic correction to scaling $c^* \sim 101N^{-2}/(\ln(N/0.4))^3$. In this range of N, the behavior is not universal and could depend on ℓ_B/b and other parameters, which requires further studies. This effective power law dependence is likely due to the interplay of logarithmic corrections from several effects, including different extent of counterion condensation, logarithmically higher electrostatic energy in comparison to classical estimates, and non-linear chain elasticity at $R/(N\sigma) > 0.5$.

We acknowledge fruitful discussions with Ralph Colby and Carlos Lopez. M. R. acknowledges financial support from National Science Foundation under Grant EFMA-1830957 and the National Institutes of Health under Grant P01-HL1088080. This work was performed, in part, at the Center for Integrated Nanotechnologies, an Office of Science User Facility operated for the U.S. Department of Energy (DOE) Office of Science. Sandia National Laboratories is a multimission laboratory managed and operated by National Technology and Engineering Solutions of Sandia, LLC, a wholly owned subsidiary of Honeywell International, Inc., for the U.S. DOEs National Nuclear Security Administration under contract DE-NA-0003525.

References

(1) Colby, R. Structure and Linear Viscoelasticity of Flexible Polymer Solutions: Comparison of Polyelectrolyte and Neutral Polymer Solutions. *Rheol. Acta* **2010**, *49*, 425–442.

(2) Dobrynin, A. V.; Rubinstein, M. Theory of polyelectrolytes in solutions and at surfaces. *Prog. in Poly. Sci.* **2005**, *30*, 1049–1118.

(3) Muthukumar, M. 50th Anniversary Perspective: A Perspective on Polyelectrolyte Solutions. *Macromolecules* **2017**, *50*, 9528–9560.

(4) Qin, J.; de Pablo, J. J. Criticality and Connectivity in Macromolecular Charge Complexation. *Macromolecules* **2016**, *49*, 8789–8800.

(5) Shen, K.; Wang, Z.-G. Electrostatic correlations and the polyelectrolyte self energy. *The Journal of Chemical Physics* **2017**, *146*, 084901.

(6) Rubinstein, M.; Colby, R. *Polymer Physics*; Oxford University Press: Oxford, 2003.

(7) de Gennes, P. *Scaling Concepts in Polymer Physics*; Cornell University: Ithaca, NY, 1979.

(8) Kaji, K.; Urakawa, H.; Kanaya, T.; Kitamaru, R. Phase diagram of polyelectrolyte solutions. *J. de Physique* **1988**, *49*, 993–1000.

(9) Boris, D. C.; Colby, R. H. Rheology of Sulfonated Polystyrene Solutions. *Macromolecules* **1998**, *31*, 5746–5755.

(10) Kuhn, W.; Künzle, O.; Katchalsky, A. Verhalten polyvalenter fadenmolekelionen in lösung. *Helvetica Chimica Acta* **1948**, *31*, 1994–2037.

(11) De Gennes, P.-G.; Pincus, P.; Velasco, R.; Brochard, F. Remarks on polyelectrolyte conformation. *J. de physique* **1976**, *37*, 1461–1473.

(12) Dobrynin, A. V.; Colby, R. H.; Rubinstein, M. Scaling Theory of Polyelectrolyte Solutions. *Macromolecules* **1995**, *28*, 1859–1871.

(13) Liao, Q.; Dobrynin, A. V.; Rubinstein, M. Molecular Dynamics Simulations of Polyelectrolyte Solutions: Nonuniform Stretching of Chains and Scaling Behavior. *Macromolecules* **2003**, *36*, 3386–3398.

(14) Stevens, M.; Kremer, K. Structure of of Salt-Free Linear Polyelectrolytes. *J. Chem. Phys.* **1995**, *103*, 1669.

(15) Hockney, R.; Eastwood, J. *Computer Simulation using Particles*; Adam Hilger: New York, 1988.

(16) Tuckerman, M.; Berne, B. J.; Martyna, G. J. Reversible multiple time scale molecular dynamics. *J. Chem. Phys.* **1992**, *97*, 1990–2001.

(17) Stevens, M. J.; McIntosh, D. B.; Saleh, O. A. Simulations of Stretching a Strong, Flexible Polyelectrolyte. *Macromolecules* **2012**, *45*, 5757–5765.

Graphical TOC Entry